Generation of Aluminum Nanoparticles Using an Atmospheric Pressure Plasma Torch

John C. Weigle,[†] Claudia C. Luhrs,[‡] C. K. Chen,[†] W. Lee Perry,[†] Joseph T. Mang,[†] Martin B. Nemer,[†] Gabriel P. Lopez,[§] and Jonathan Phillips*[,†,§]

Los Alamos National Laboratory, P.O. Box 1663, Los Alamos, New Mexico 87545, Department of Chemistry, University of Guadalajara, Blvd. Marcelino Garcia, Barragan 1421, Guadalajara, Jalisco, Mexico 44480, and Department of Chemical and Nuclear Engineering, University of New Mexico, Albuquerque, New Mexico 87131

Received: February 9, 2004; In Final Form: September 7, 2004

Nanoparticles of aluminum metal were generated by passing an aerosol of micrometer-scale (mean 50 μm) particles in argon through an atmospheric pressure plasma torch operated at less than 1000 W. A designed experiment was conducted to investigate the effects of plasma gas flow rate, aerosol gas flow rate, and applied power on the shape, size, and size distribution of the final particles. The size and shape of the metal particles were dramatically impacted by the operating parameters employed. At relatively low powers or at high powers and short residence times, virtually all the particles are spherical. Under other conditions, the particles had spherical heads, and virtually all had tails, some quite long. The particle size distributions also were influenced by the operating conditions. Under most conditions the size distributions were log-normal, consistent with growth by agglomeration. However, under some conditions, the population of particles above or below the mode was far too great to be consistent with a log-normal distribution. For example, the particle distributions tend to show an unusual concentration of very small particles at relatively short residence times and low aluminum feed rates. The distributions tend to show an unusual concentration of large particles at relatively long residence times and high aluminum feed rates. On the basis of the data collected, some simple models of the mechanism of nanoparticle formation were postulated which should be of value in future studies of the process.

Introduction

The broad interest in nanostructures has spurred development of a number of techniques for creating metallic nanoparticles. Among the methods developed to make metallic nanoparticles are metal gas evaporation,[1,2] metal evaporation in a flowing gas stream,[3,4] mechanical attrition,[5] sputtering,[6] electron beam evaporation,[7] electron beam induced atomization of binary metal azides,[8] expansion of metal vapor in a supersonic free jet,[9] inverse micelle techniques,[10] laser ablation,[11] laser-induced breakdown of organometallic compounds,[12] pyrolysis of organometallic compounds,[13] and microwave plasma decomposition of organometallic compounds.[14,15] In our laboratory, we recently developed a novel method[16] in which micrometer-scale metal particles are sent as an aerosol, using an inert gas carrier, through a low-power, atmospheric pressure plasma, referred to as the aerosol through plasma (ATP) method.

A cost-effective method should continuously produce pure metallic nanoparticles with tight specifications, and should employ relatively inexpensive precursor materials. Although some of the above methods fulfill some of these criteria, none have been scaled up to a viable commercial process. Thus, the development of a truly superior method for generating uniform, high-purity, metallic nanoparticles on a large scale remains an open challenge. At this point the relative advantages and disadvantages of the various approaches are far from clear. For example, although it is known that nanoparticles can be produced continuously from inexpensive precursors using the ATP technique, so that it meets some of the noted requirements for commercialization, the mechanism of particle growth remains unclear, and the impact of the operating conditions on the size and shape of the particles has not been investigated. This information is critical for engineering analysis and scaleup.

As a first step in understanding the mechanism of nanoparticle formation using the ATP approach, we have studied the formation of aluminum nanoparticles from micrometer-scale aluminum particles fed as an aerosol through an atmospheric pressure, low-power (<1000 W), microwave-generated argon plasma. Variations in the operating parameters of the process impacted the particle size distribution and shape of the nanoparticles that formed. This information in turn provided a basis for suggesting a mechanism for nanoparticle formation.

Two findings were particularly surprising. First, although under most conditions the particles that formed were spherical, under certain operating conditions many of the particles had tails. We postulate that the tails form as a consequence of rapid cooling of the outer shell of the particles, and the ejection of the remaining molten metal to form the tail. Second, three distinct types of particle size distributions were found. Under most conditions the particle size distributions were easily fit as log-normal. This suggests that the dominant growth process (following a nucleation process) was agglomeration. However, under some conditions the particle size distribution clearly was not consistent with growth by a normal agglomeration process. A significant excess of particles was found for particle sizes above or below the mode of the distribution.

* To whom correspondence should be addressed at the Los Alamos National Laboratory. E-mail: jphillips@lanl.gov. Phone: (505) 665-2682. Fax: (505) 665-5548.

[†] Los Alamos National Laboratory.

[‡] University of Guadalajara.

[§] University of New Mexico.

10.1021/jp049410q CCC: $27.50
Published on Web 11/06/2004

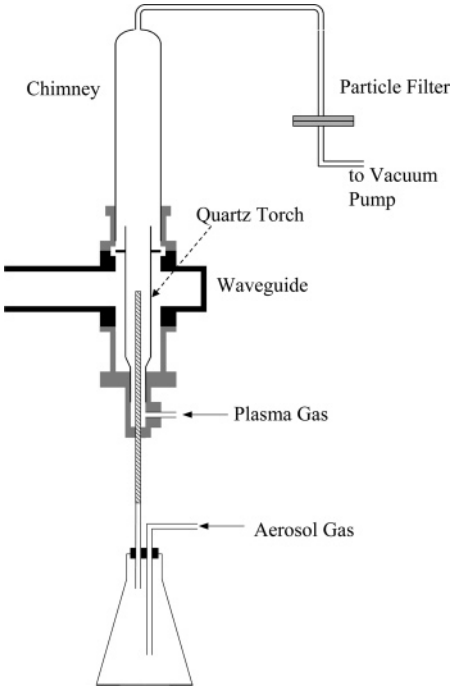

Figure 1. Schematic diagram of the coupler, torch, and chimney of the microwave plasma system (not to scale).

We believe there are two possible mechanisms that contribute to the presence of excess small particles. The first possibility is that particle nucleation, creating very small particles that grow via Ostwald ripening, occurs concomitantly with agglomeration. The second possibility is that repulsion between charged particles prevents agglomeration of the particles beyond a certain diameter, thus tending to create distributions with a maximum particle size. The existence of distributions with large particle branches cannot be readily explained by either inertial forces or electrostatic repulsion. This indicates a need to produce more detailed information regarding particle velocity distributions, particle charging, and other features of particle behavior in atmospheric pressure plasmas.

Finally, we found it necessary to explore a frequent, and surprising, postulate in the literature of particle growth in plasmas: particles carrying like charges do not grow by agglomeration. A simple analysis of the energetics of particle interaction shows that electrostatic repulsion influences the collision rate of two submicronmeter-sized particles, but the precise manner is a function of the kinetic energy of the particles. Particles with sufficient kinetic energy can and will overcome repulsion effects.

Experimental Section

In most key respects the method used to make nanoparticles in this study is similar to the methods used to make large spherical ceramics via the agglomeration of small, irregularly shaped ceramic particles of the same composition,[17] to make micrometer-scale spherical BN particles from input micrometer-scale platelet particles of BN,[18] or to make supported metal catalysts.[19] Figure 1 shows a schematic of the microwave plasma system, and detailed descriptions of the plasma torch are available in the earlier papers.

In essence, the ATP technique consists of the following four steps: (1) Generate a cloud of precursor particulates. For this study, this was done by agitating a 25 mL flask containing irregularly shaped, micrometer-sized (10−80 μm) aluminum (99.99%) from Silverline Corp. in an ultrasonic bath, and impinging ultra-high-purity argon onto the flask bottom. (2) Direct the aerosol flow into the center of the waveguide (approximately 5 cm in height) with a 3 mm i.d. alumina tube that terminates in the center of the waveguide. (3) Direct the plasma gas (also ultra-high-purity argon) through the annular region between the outside of the quartz torch (19 mm o.d.) and the alumina tube. (4) Collect the transformed particles using a 0.45 μm filter at the end of a Pyrex chimney (40 mm i.d. by 25 cm height), affixed to the waveguide with a Viton O-ring and clamp.

TABLE 1: Designed Experiment Operating Conditions and Measured Feed Rates

sample	plasma gas flow (slpm)	aerosol gas flow (slpm)	power (W)	Al feed rate (mg/h)
A	1.0	0.5	500	96
B	1.0	0.5	500	454
C	1.0	0.5	1000	520
D	1.0	1.0	500	283
E	1.0	1.0	1000	981
F	1.0	1.0	1000	702
G	3.5	0.5	500	356
H	3.5	0.5	1000	170
I	3.5	0.5	1000	167
J	3.5	1.0	500	854
K	3.5	1.0	1000	904
L	2.25	0.75	750	510

The desired product determines the gases used and operating conditions employed. For example, the gases must be inert (Ar or He) to make metallic product. To make nanoparticles, it is necessary to adjust the flow rates and absorbed power sufficiently to fully atomize the precursor particles in the aerosol. In contrast, to grow ceramic particles by agglomeration,[17] an oxidizing gas (air or O_2) is used, and operating conditions are selected to ensure that the precursor particles melt, but do not decompose or atomize. Clearly, for the present work we focused on creating conditions that met the former set of requirements.

The program design was a three-factor, two-level designed experiment with three repeats and one midpoint. The three factors chosen were the plasma gas flow rate, the aerosol gas flow rate, and the applied power. Table 1 summarizes the conditions tested. The "low" levels of the aerosol gas and plasma gas flows (0.5 and 1.0 slpm, respectively) were established at the minimum controllable flow rates for the two streams. The "high" level of the aerosol gas flow was selected on the basis of the stability of the plasma. That is, at higher aerosol gas flow (higher particle feed rate) the plasma could not be maintained. The high level of the plasma gas was selected so that the flame was contained within the chimney. Finally, the power levels (500 and 1000 W) were selected on the basis of the minimum power necessary to maintain a stable plasma and the maximum sustainable operating power of the microwave generator.

Analysis of the final particles that formed was performed using a JEOL 2010 operating at 200 kV transmission electron microscope with point-to-point resolution of 0.19 nm, located in the Department of Earth and Planetary Sciences at the University of New Mexico. Both energy dispersive spectroscopy (EDS) and visual inspection clearly demonstrated that the particles were primarily metallic as formed. EDS also showed increasing oxygen concentrations in the particles as they aged. Pictures taken with this microscope were used to determine the particle size distributions using NIH Image software. At least 500 particles were counted for each distribution, and the best log-normal fit parameters were determined by minimizing the sum of the squares of the error between the predicted and observed distributions. As the effective resolution of the images (1 nm) was far smaller than the bin size (5 nm), it is clear the

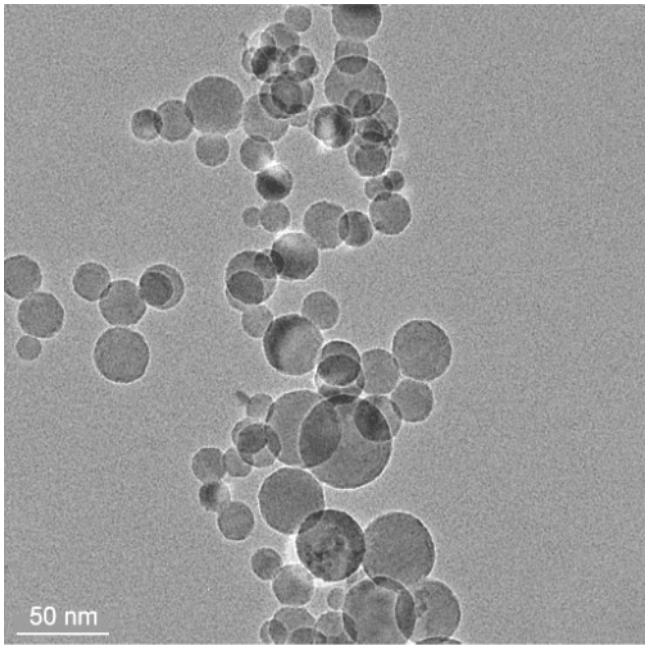

Figure 2. Spherical particles formed in the plasma torch, sample A.

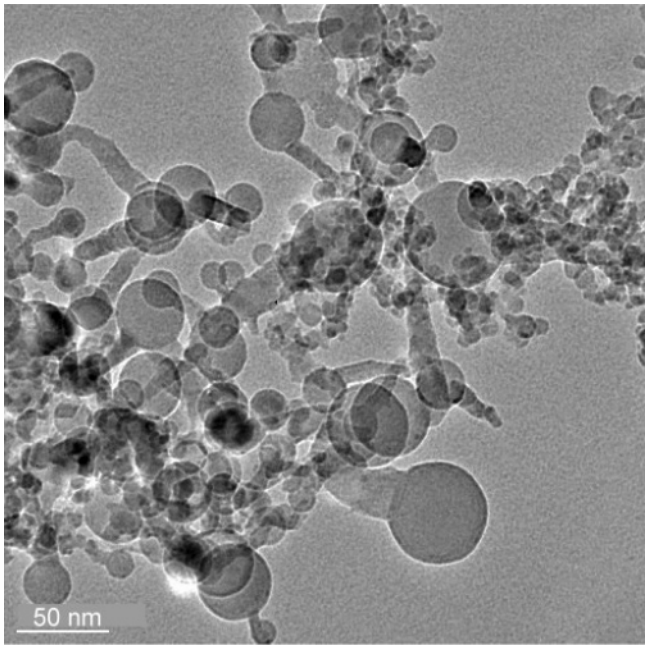

Figure 3. Aluminum nanoparticles that formed tails upon solidification, sample D.

counting was accurate. In those cases in which a superabundance of particles in the 0−5 nm range was detected, smaller bin size (2.5 nm) counting was also conducted. No significant change in the shape of the particle size distribution was detected. Particle size distributions were also analyzed at Los Alamos National Laboratory using small-angle X-ray scattering (SAXS).[20−22]

Results

TEM analysis of the particles collected on filter paper downstream from the chimney indicated that plasma operating conditions significantly impacted not only the average size of the aluminum particles that formed, but the character of the particle size distribution and the shape of the particles.

Examples of spherical particles that form under specific conditions are shown in Figure 2. Spherical particles are presumed to form when a metal liquid drop is rapidly frozen. Under other conditions, particles with distinct tails were found to form, as seen in Figure 3. The tails were presumed to form when the particle exteriors froze, leaving molten metal cores that burst out and subsequently froze. This mechanism is elaborated upon in the Discussion. In Table 2 the average particle size, nature of the particle size distribution, and notes on the shapes of the particles produced are all presented.

Three distinct particle size distribution (PSD) types were observed. Most of the experiments yielded particles that fit a log-normal distribution. However, some operating conditions yielded particles that had more small particles (<5 nm) than would be predicted by the log-normal distribution. Other operating conditions yielded particles that had more large particles (>50 nm) than predicted by the log-normal distribution.

In most cases, the distributions were fit well by a log-normal distribution (Figure 4a). The only variations were in the average particle size observed and the value of the normalized σ value. In fact, for particles with these distributions the sizes were narrowly distributed, as evidenced by the low values of σ. Particle size distributions of this type are associated with growth dominated by the agglomeration process.[23−26] Also, in those cases in which a superabundance of small particles was detected, particle distributions with nearly the same average particle size, but without the superabundance effect, were found to form under different operation conditions. For example, compare distribution I with distributions H and K in Table 2.

The sizes of the particles with tails were determined by the distribution of the diameters of only the head section of such particles. Only the heads were considered in determination of particle sizes, because, as discussed below, it is believed that the particles were initially spherical. Thus, comparisons based on this measurement are a valid means to compare the size of particles with tails with the size of particles that remained spherical.

The second type of particle size distribution observed was only quasi-log-normal, because the small particle population was too high to be consistent with the log-normal distribution. That is, the section of the distribution greater than the mode could be readily fit as log-normal. However, the portion of the distribution lower than the mode did not sharply drop toward zero (Figure 4b). In all of these distributions, there were far more small particles than predicted by growth via agglomeration. The excess small particles were quantified as the difference between the predicted and observed small particle populations. This result implies a modified growth mechanism. Two suggestions for growth process modification are presented in the following section.

The third type of particle size distribution observed was also quasi-log-normal, but in this case the particles smaller than the mode are fit well by the log-normal distribution, while the population of large particles (>50 nm) is higher than would be predicted by a simple log-normal distribution (Figure 3c). The large particles cannot be attributed to small precursor particles simply passing through the torch. The precursor particles had an initial size range of 10−80 μm; thus, the "large" product particles had diameters less than one-tenth the diameter of the smallest precursor particles. Therefore, these particles must be formed within the torch rather than result from particle "bypass".

The PSDs measured via SAXS agreed well with the distributions determined via TEM measurements. Figure 5 shows the distributions measured for three samples via SAXS, and Table 3 compares the average particle sizes determined from SAXS to those determined from TEM. SAXS results were analyzed

TABLE 2: Particle Size Distributions and Descriptions

sample	mean particle size (nm)	$\sigma(\ln x)$	comments
A	21.3	0.55	spherical particles; a small particle branch is present relative to a log-normal PSD
B	34.2	0.58	spherical particles; a large particle branch is present relative to a log-normal PSD
C	34.1	0.54	spherical particles; a large particle branch is present relative to a log-normal PSD
D	11.2	0.85	tails on particles; log-normal
E	17.0	0.61	spherical particles; log-normal
F	14.6	0.41	spherical particles; log-normal
G	16.4	0.47	spherical particles; log-normal
H	11.1	0.59	spherical particles; log-normal
I	7.4	0.42	spherical particles; a small particle branch is present relative to a log-normal PSD
J	16.7	0.44	spherical particles; log-normal
K	7.8	0.53	spherical particles; log-normal
L	9.0	0.43	tails on particles; a small particle branch is present relative to a log-normal PSD

according to a metal core-oxide shell model. The average particle sizes determined by each method are in good agreement. Moreover, both techniques produced distributions that varied from log-normal when an excess of large particles were present. A large particle "branch" is clearly present in the SAXS measurements of samples B and C.

Discussion

The basic mechanism of nanoparticle formation in the ATP method is postulated to be a three-step process. First, the micrometer-scale aluminum particles atomize when the aerosol enters the hot zone of the torch. The temperature of the afterglow of similar plasmas was measured to be about 3500 K, suggesting that inside the coupler the temperature is far higher, certainly on the order of 4000 K,[27] a temperature expected not simply to melt aluminum, but to vaporize it. Second, the metal gas is carried by convection to a cooler area of the plasma; on the basis of earlier temperature profile measurements, this is probably at least 2 cm above the top of the coupler.[27] The temperature is not known, but likely to be lower than the vaporization temperature of aluminum ($T_{vap} = 2329$ K).[28] Like any other supercooled phase, a new phase begins to form by homogeneous nucleation, a process generally believed to lead to the formation of spherical primary particles.[24−26] The third step, agglomeration, begins immediately upon the formation of liquid nuclei. It halts once the particles reach a temperature lower than the melting temperature of aluminum ($T_f = 933$ K).[28]

This postulated mechanism is probably not complete, since the results pose several questions not readily answered by the model. First, given that the mechanism of particle formation and growth is assumed similar in all cases, why are the particle size distributions and particle shapes not the same in all cases? Second, why are the particles spherical in some cases, and why do they have tails in others? Third, why is a small particle branch present in some of the distributions, and a large particle branch in others?

The question of the changes in shape can be answered by assuming that the tails form when the outer layer of the particles freezes before the inside, and that this leads to a breakout of molten metal, followed by freezing of the ejected material. It is well-known that surface tension effects, thermal contraction, and density differences between the solid and liquid phases can lead to high pressures in the liquid core of a solidifying sphere.[29−34] Small spheres (<200 nm diameter) can be subjected to large, positive internal pressure. Hsiao et al.[31] provide a model describing the rupture of the solid shell due to tangential stresses induced by the pressurization.

Our conceptual model is fully consistent with these previous studies, and with all current experimental observations. For example, it can be shown that the mass in the tails never exceeds the mass present in the original spherical drop. Specifically, assuming the tails are solid masses of conical shape, it is possible to compute the maximum cone height. Table 4 summarizes the fraction of mass present in the tails versus the corresponding spheres for some of the particles shown in Figure 3. Clearly, only a small fraction of the mass originally present in those spheres ends up as part of the tail.

If the particle tails do indeed form from the molten interior of a particle breaking through the solid shell, the interior of the particle head may be hollow. This hypothesis brings up a related question: Does a hollow sphere have a distinct appearance in TEM? That is, if the tailed particles are hollow, should they have an appearance different from that of the nontailed spheres? According to the model for tail formation provided above, the particles with tails are partially hollow. Yet the TEM images of the particle heads are indistinguishable from the tailless particles, which are presumably solid spheres.

The historical record of the subject suggests that it is very difficult to distinguish hollow metal particles from solid metal particles using TEM. For example, there is a long history of confusion regarding the structure of hollow spherical supported FeMn particles. Initially, the TEM images were interpreted to arise from either pitted or torroidal shapes.[35−38] Detailed studies of individual particle shapes and volumes before and after oxidation were necessary to demonstrate that the TEM images arose from hollow particles.[39] Thus, we feel it is reasonable to postulate that it is virtually impossible to distinguish solid and hollow aluminum nanoparticles using TEM.

Understanding the deviations of the particle size distributions from log-normal requires examining the particle dynamics within the torch. The first potential source of the smallest size particles would be the continued generation of atomic aluminum while agglomeration is taking place. It is plausible that particles, even larger ones formed by agglomeration, pass through zones in which the temperature is hot enough to reablate the surface. This would lead, yet further downstream, to nucleation of very small particles. A detailed mechanistic model demonstrates this type of distribution is found in soot particles when nucleation kinetics are dominated by atomic-scale processes, even as larger particles are growing by agglomeration.[40] Indeed, earlier maps of temperature profiles in the afterglow of plasmas of the type used in this study indicate that the profiles can be quite complex, and can be influenced by the presence of particles.[27]

The second possible explanation for the deviations from log-normal distributions, both excess small particles and excess large particles, is due to inhibition of the growth of small particles because of drag, particle charging effects, or both. In microwave plasmas, the mobility of electrons is much higher than that of the positive ions, leading to the accumulation of negative charge, and concomitantly negative potential, on all particle surfaces.[41−49]

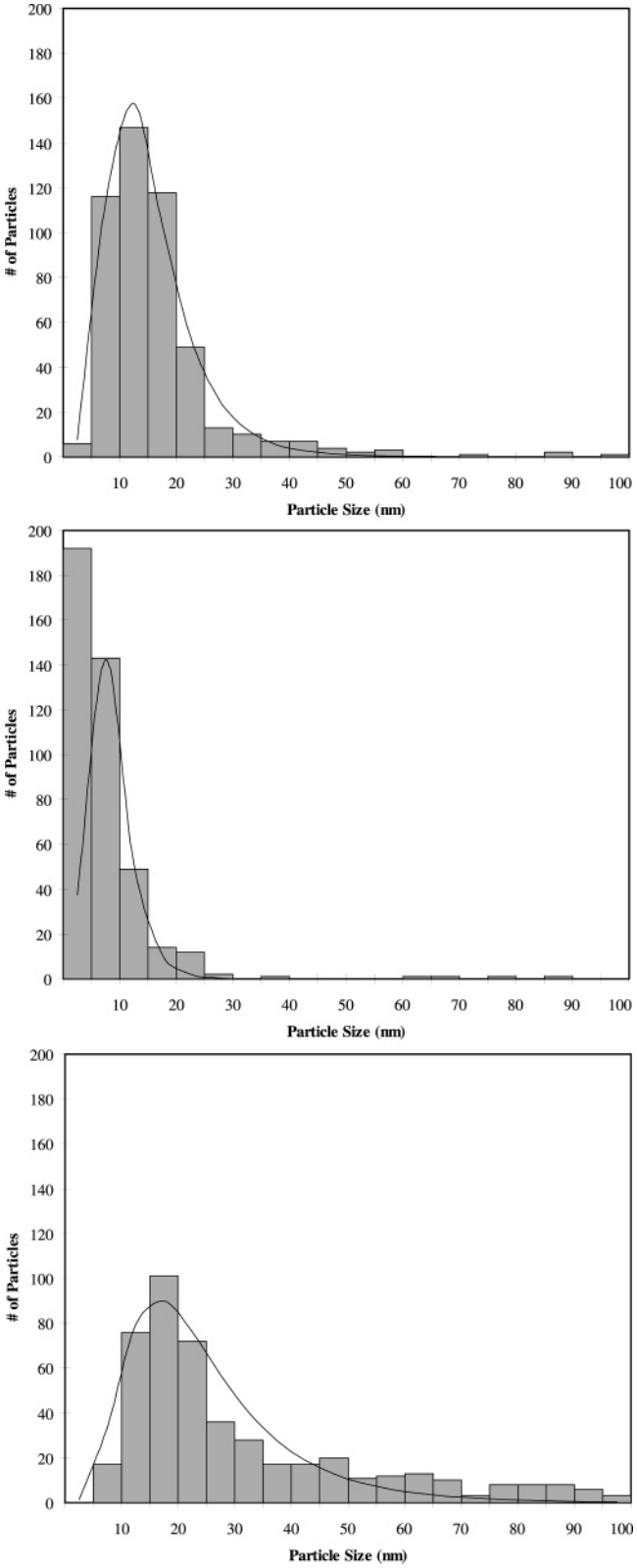

Figure 4. Various types of particle size distributions formed in the plasma torch: (a, top) log-normal distribution, sample G; (b, middle) non-log-normal distribution showing more small particles than expected, sample I; (c, bottom) non-log-normal distribution showing more large particles than expected, sample C.

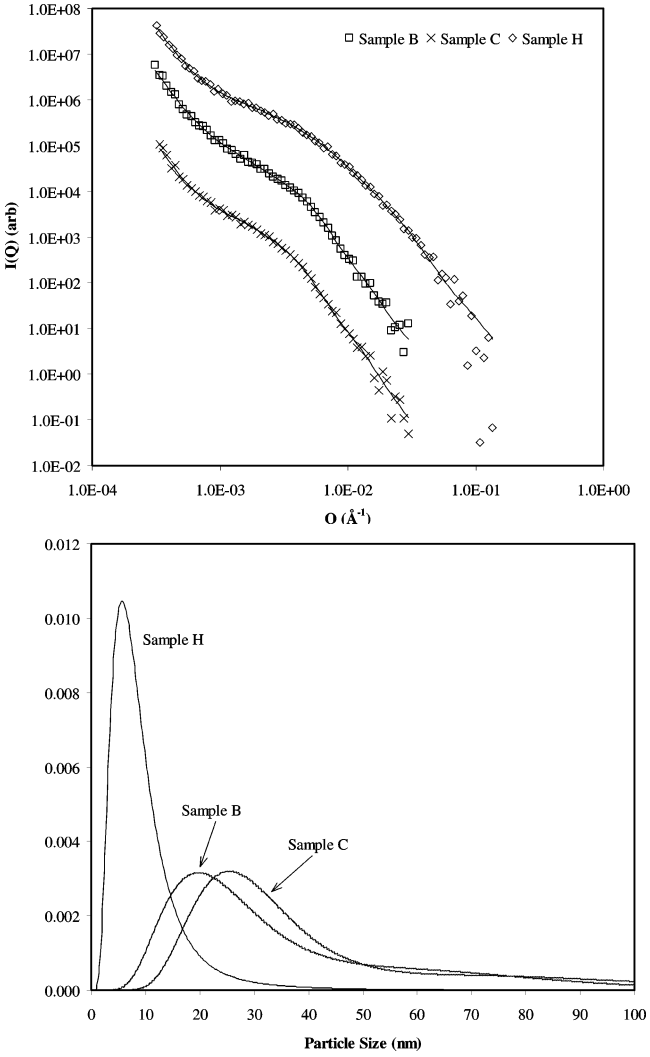

Figure 5. SAXS results. (a, top) Intensity versus momentum transfer for samples B, C, and H. The initial power-law falloff of the data is indicative of large-scale particle agglomerates, and the broad shoulders in the curves arise from distinct populations of particles. The position of the shoulder along the *Q*-axis is indicative of the average size of the particle. (b, bottom) Size distributions of the particle core for samples B, C, and H.

TABLE 3: Comparison of TEM Image Analysis and SAXS Results

sample	av particle size, TEM (nm)	av particle size, SAXS (nm)
B	34.2	36.8
C	34.1	43.6
H	11.1	9.8

TABLE 4: Volume Analysis of Particles with Tails, Sample D[a]

particle number	head vol (nm^3)	tail vol (nm^3)	particle number	head vol (nm^3)	tail vol (nm^3)
1	134000	21800	6	6500	900
2	32100	5200	7	13900	1100
3	39700	5000	8	3200	600
4	111000	17500	9	18300	1900
5	13900	2000	10	9100	1000

[a] The tails were assumed to be conical.

In an earlier paper we developed a simple model of the impact of electrostatic repulsion on the possibility of collision between two particles of the same size.[47] The particles are spherical and carry the same amount of charge. The amount of charge on the particles in the plasma can be calculated by the method provided by Matsoukas and co-workers.[41−43] The kinetic energy required to overcome the electrostatic repulsion, and thus to allow any two like-charged particles to collide, is estimated by

integrating the repulsion force between them along the path from infinity to the collision point. Once the relative velocity of the particles is established, the model provides a bound on the size of particles that will not collide and agglomerate due to surface charge induced repulsion.

Although our earlier model was the first to show that particles with like charge can collide and agglomerate under appropriate conditions of relative velocity, we failed to discuss viscous drag, a second factor that may inhibit collisions or enhance the effect of electrostatic forces. However, as shown below, viscous drag does not play a significant role in nanoparticle growth in plasma systems. Specifically, in the high-temperature environment of the plasma torch it is clear that viscosity is low and hence the Stokes number is high for submicrometer-scale particles, and hence, drag forces play an insignificant role in the growth of nanometer-sized particles.

In contrast, earlier models[48−51] that took into account the effect of particle charging assumed the particles are in a high-viscosity environment, and thus concluded that particle inertia is dissipated by drag before a collision occurs. Under this assumption, Fuchs[49] showed that the collision frequency scales exponentially with the product of particle charge, $\exp(-q_1q_2)$, and hence only a small amount of like charge is necessary to prevent particle collisions. Thus, they concluded that like-charged particles rarely collide. We believe this result is only a special case. As shown below, for particles growing in a low-drag environment (e.g., a plasma torch), particle inertia is large compared to viscous forces except for particles between about 1 and 10 μm. Hence, nanoscale particles with like charge can collide and agglomerate, inhibited only if they have insufficient kinetic energy to overcome integrated electrostatic repulsion.

The key parameter in determining whether particle inertia or viscous drag has a significant affect on collision rates is the Stokes number:

$$St = \frac{mU}{\bar{b}D} \tag{1}$$

where m is the reduced particle mass, U is the relative velocity of the pair, $\bar{b} = (b_1m_2 + b_2m_1)/(m_1 + m_2)$ is the reduced viscous drag (b_i and m_i are the drag and mass of each particle), and D is the reduced particle diameter. Possible mechanisms of relative particle transport in the plasma include random thermal motion, shear flow, buoyancy, and thermophoresis. Estimating these velocities shows that random thermal motion is dominant, $U_T = (8kT/\pi m)^{1/2}$, under the conditions employed in this study, where k is the Boltzmann constant and T is assumed to be the melting temperature of aluminum (933 K).

The drag must be calculated to estimate the Stokes numbers for our experiments. In rarified gas flow, the lubrication resistance between two particles in near-contact motion has been shown to be at most log−log singular[52] close to contact, and is too weak to prevent van der Waals attraction from causing coalescence. Thus, a Stokes number based on infinite separation is a reasonable choice for the scaling arguments made herein. The drag on each particle is calculated from $b_i = 3\pi\mu D_i/C_c[Kn_i]$, where D_i is the diameter of each particle, the gas viscosity is estimated at 10^{-4} P, and $C_c[Kn_i]$ is the Cunningham correction factor as a function the Knudsen number.[53] Typical values of the Stokes number are shown in Figure 6. Clearly, in our plasma, the Stokes number is large, except for particles between 1 and 10 μm in diameter. Consequently, drag forces are insignificant for the particles of interest in this work, and the only forces that need to be considered are those of electrostatic repulsion.

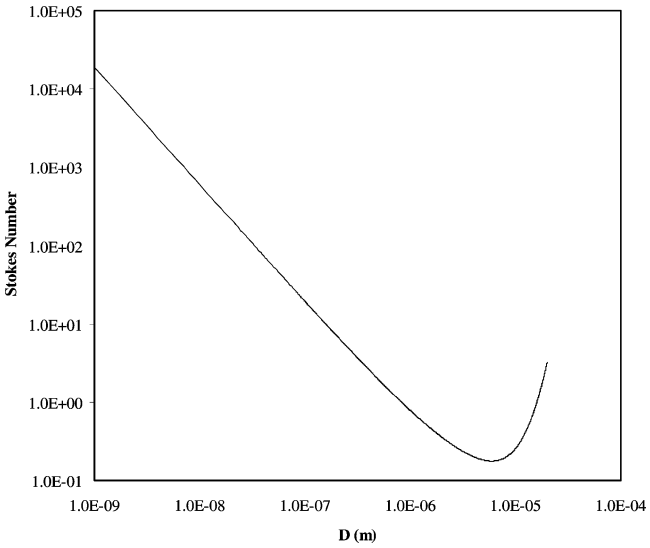

Figure 6. Effect of particle size on the Stokes number. Note that drag forces are only important for particles in the 1−10 μm range.

For particles larger than 10 μm, both drag forces and electrostatic forces may play a role.

In our earlier model, electrostatic repulsion becomes insignificant above a certain maximum particle size. However, in that analysis it was postulated that all particles have the same relative velocity, regardless of size. In this study we assume that all particles have the same kinetic energy, which is consistent with the thermal velocity model. This means that larger particles have smaller velocities relative to other particles; hence, the collision velocity decreases with increasing particle size. As shown below, this dramatically increases the effectiveness of charge repulsion on reducing particle collisions and agglomeration. In turn, this finding leads to a surprising conclusion: Neither drag forces nor electrostatic repulsion can explain the existence of large particle branches found in some experiments.

The work required to bring two particles together against the repulsion created by surface charge can be written as

$$W_{el} = \epsilon_0 V^2 D\pi(2 - \log[4])$$

where the plasma potential, V, is defined by Matsoukas[41] to be

$$V = 3kT_e/e$$

Assuming the thermal model of particle velocity yields a particle kinetic energy independent of size ($3kT_r$). Hence, the energy required to overcome electrostatic repulsion, relative to the particle kinetic energy, can be written

$$W_{el}/3kT_r = \frac{9\epsilon_0 kT_e^2 D\pi(2 - \log[4])}{T_r^2 e^2}$$

From this equation and the stated assumptions, electrostatic repulsion effectively increases linearly with particle diameter. Thus, above a given minimum size, electrostatic repulsion prevents particle agglomeration. Assuming an electron temperature of 1 eV and a particle temperature equal to the melting temperature of aluminum, only particles smaller than about 1 nm in diameter have sufficient energy to collide. Assuming a higher particle temperature and a lower electron temperature increases the maximum size at which agglomeration can occur, but that size is at most a few tens of nanometers.

Therefore, electrostatic repulsions should produce kinetics in which small particles grow much more rapidly than large particles. Such a system would not yield log-normal particle distributions, but rather particle distributions with maximum particle size cutoffs. This may partially account for particle size distributions with a small particle branch (samples A, I, and L), but not large particle branches (samples B and C) in which it is clear large particles are growing faster than small particles. The mechanism by which electrostatic repulsion creates the small branch follows from the model presented above. The work required to overcome electrostatic repulsion is lowest for small particles, and only small particles have the kinetic energy to overcome this repulsion. Thus, the number of particles above some cutoff value should decrease more sharply than in a log-normal distribution.

Neither drag nor electrostatic repulsion effects can explain the presence of a large particle branch. Modifications in the assumptions are required. For example, charge may bleed off large particles in the low-temperature portion of the afterglow, where agglomeration of liquid particles can take place. Alternatively, large particles may have higher collision velocities than those predicted by the thermal velocity model. One potential source for higher velocity is the presence of eddy currents within the torch. To avoid speculative analysis, it is clearly desirable to make more detailed measurements of the plasma structure and particle velocity profiles.

Conclusion

The influence of operating parameters on the size, size distribution, and shape of aluminum nanoparticles formed using an ATP method was explored. Under most conditions, spherical particles with a log-normal size distribution and small σ values were formed. This observation is consistent with particle formation and growth via the following mechanism. First, precursor particles are completely vaporized in the hottest region of the torch. Second, homogeneous nucleation and agglomeration occur in the cooler afterglow region. In some cases, either a small or a large branch—relative to a log-normal distribution—was measured in the particle size distribution. Electrostatic repulsion resulting from particle charging may be responsible for the existence of the small branch. Another explanation for the size distributions with a small particle branch is the continuous ablation of the particles, and subsequent formation of additional primary particles. The effects of drag forces on particles smaller than 1 μm can readily be discounted. An explanation for the existence of distributions with large particle branches was not found. Using standard assumptions for particle velocities and particle charging led to the conclusion that neither drag effects nor repulsions between particles with like charges could explain this observation.

Most of the particles were spherical, although some formed tails, presumably when the liquid core of a solidifying particle broke through the solid shell. Correlations between the particle size distributions and the operating conditions were weak; however, distributions with excess small particles seemed to form at lower aluminum feed rates and shorter residence times. Distributions with excess large particles seemed to form at higher aluminum feed rates and longer residence times.

Acknowledgment. Funding for this work was provided by Los Alamos National Laboratory and the DOE through the US/Mexico Materials Corridor Initiative.

References and Notes

(1) Kimoto, K.; Kamiya, Y.; Nonoyama, M.; Uyeda, R. *Jpn. J. Appl. Phys.* **1963**, *2*, 702−713.
(2) Gong, W.; Li, H.; Zhao, Z. G.; Chen, J. C. *J. Appl. Phys.* **1991**, *69*, 5119−5121.
(3) Iwama, S.; Hayakawa, K. *Nanostruct. Mater.* **1992**, *1*, 113−118.
(4) Panda, S.; Pratsinis, S. E. *Nanostruct. Mater.* **1995**, *5*, 755−767.
(5) Fecht, H. J. *Nanostruct. Mater.* **1992**, *1*, 125−130.
(6) Haas, V.; Birringer, R. *Nanostruct. Mater.* **1992**, *1*, 491−504.
(7) Eastman, J. A.; Thompson, L. J.; Marshall, D. J. *Nanostruct. Mater.* **1993**, *2*, 377−382.
(8) Herley, P. J.; Jones, W. *Nanostruct. Mater.* **1993**, *2*, 553−562.
(9) Recknagle, K.; Xia, Q.; Chung, J. N.; Crowe, C. T.; Hamilton, H.; Collins, G. S. *Nanostruct. Mater.* **1994**, *4*, 103−111.
(10) Chen, J. P.; Sorensen, C. M.; Klabunde, K. J.; Hadjipanayis, G. C.; Devlin, E.; Kostikas, A. *Phys. Rev. B* **1995**, *51*, 11527−11532.
(11) Yamamoto, T.; Mazumder, J. *Nanostruct. Mater.* **1996**, *7*, 305−312.
(12) Majima, T.; Miyahara, T.; Haneda, K.; Ishii, T.; Takami, M. *Jpn. J. Appl. Phys.* **1994**, *33*, 4759−4763.
(13) Sawada, Y.; Kageyama, Y.; Iwata, M.; Tasaki, A. *Jpn. J. Appl. Phys.* **1992**, *31*, 3858−3861.
(14) Chou, C. H.; Phillips, J. *J. Mater. Res.* **1992**, *7*, 2107−2113.
(15) Brenner, J. R.; Harkness, J. B. L.; Knickelbein, M. B.; Krumdick, G. K.; Marshall, C. L. *Nanostruct. Mater.* **1997**, *8*, 1−17.
(16) Phillips, J.; Perry, W. L.; Kroenke, W. U.S. Patent 6,689,192.
(17) Chen, C. K.; Gleiman, S.; Phillips, J. *J. Mater. Res.* **2001**, *16*, 1256−1265.
(18) Gleiman, S.; Chen, C. K.; Datye, A.; Phillips, J. *J. Mater. Sci.* **2002**, *37*, 3429−3440.
(19) Shim, H.; Phillips, J.; Fonseca, I. M.; Carabineiro, S. *Appl. Catal.* **2002**, *237*, 41−51.
(20) Glatter, O.; Kratky, O. *Small Angle X-Ray Scattering*; Academic Press: London, 1982.
(21) Rieker, T. P.; Hubbard, P. F. *Rev. Sci. Instrum.* **1998**, *69*, 3504−3509.
(22) Pedersen, J. S. *Adv. Colloid Interface Sci.* **1997**, *70*, 171−210.
(23) Wu, N. L.; Phillips, J. *J. Catal.* **1988**, *113*, 129−143.
(24) Frenklach, M.; Harris, S. J. *J. Colloid Interface Sci.* **1987**, *118*, 252−261.
(25) Frenklach, M.; Wang, H. In *Soot Formation in Combustion: Mechanisms and Models*; Bockhorn, H., Ed.; Springer-Verlag: Berlin, 1994; pp 162−190.
(26) Haynes, B. S.; Wagner, H. G. *Prog. Energy. Combust. Sci.* **1981**, *7*, 229−273.
(27) Chen, C. K.; Phillips, J. *J. Phys. D: Appl. Phys.* **2002**, *35*, 998−1009.
(28) *Perry's Chemical Engineers' Handbook*, 6th ed.; Perry, R. H., Green, D., Eds.; McGraw-Hill: New York, 1984.
(29) Campbell, J. *Trans. Metall. Soc. AIME* **1967**, *239*, 138−142.
(30) Campbell, J. *Trans. Metall. Soc. AIME* **1968**, *242*, 264−268.
(31) Hsiao, K. H.; Cox, J. E.; Hedgcoxe, P. G.; Witte, L. C. *J. Appl. Mech.* **1972**, *39*, 71−77.
(32) Wray, P. J. *Metall. Trans.* **1974**, *5*, 2602−2603.
(33) Forgac, J. M.; Schur, T. P.; Angus, J. C. *J. Appl. Mech.* **1979**, *46*, 83−89.
(34) Forgac, J. M.; Angus, J. C. *Metall. Trans. B* **1981**, *12*, 413−416.
(35) Chakraborti, S.; Datye, A. K.; Long, N. J. *J. Catal.* **1987**, *108*, 444−451.
(36) Arai, M.; Nakayama, T.; Nishiyama, Y. *J. Catal.* **1988**, *111*, 440−444.
(37) Ruckenstein, E.; Chen, J. J. *J. Colloid Interface Sci.* **1982**, *86*, 1−11.
(38) Tatarchuk, B.; Chludzinski, J. J.; Sherwood, R. D.; Dumesic, J. A.; Baker, R. T. K. *J. Catal.* **1981**, *70*, 433−439.
(39) Chen, A. A.; Vannice, M. A.; Phillips, J. *J. Catal.* **1989**, *116*, 568−585.
(40) Zhao, B.; Yang, Z.; Johnston, M. V.; Wang, H.; Wexler, A. S.; Balthasar, M.; Kraft, M. *Combust. Flame* **2003**, *133*, 173−188.
(41) Matsoukas, T.; Russell, M. *J. Appl. Phys.* **1995**, *77*, 4285−4292.
(42) Matsoukas, T.; Russell, M.; Smith, M. *J. Vac. Sci. Technol., A* **1996**, *14*, 624−630.
(43) Lee, K.; Matsoukas, T. *J. Appl. Phys.* **1999**, *85*, 2085−2092.
(44) Kim, K. S.; Kim, D. J. *J. Appl. Phys.* **2000**, *87*, 2691−2699.
(45) Kim, D. J.; Kim, K. S. *AIChE J.* **2002**, *48*, 2499−2509.
(46) Kim, K. S.; Kim, D. J.; Yoon, J. H.; Park, J. Y.; Watanabe, Y.; Shiratani, M. *J. Colloid Interface Sci.* **2003**, *257*, 195−207.
(47) Vanamu, G.; Lester, K.; Datye, A. K.; Weigle, J. C.; Chen, C. K.; Kelly, D.; Phillips, J. *AIChE J.* **2004**, *50*, 2090.
(48) Choi, S. J.; Kushner, M. J. *J. Appl. Phys.* **1994**, *75*, 3351−3357.
(49) Fuchs, N. A. *The Mechanics of Aerosols*; Pergamon Press: Oxford, 1964.
(50) Maisels, A.; Kruis, F. E.; Fissan, H. *J. Colloid Interface Sci.* **2002**, *255*, 332−340.
(51) Kortshagen, U.; Bhandarkar, U. *Phys. Rev. E* **1999**, *60*, 887−989.
(52) Sundararajakumar, R. R.; Koch, D. L. *J. Fluid Mech.* **1996**, *313*, 283−308.
(53) Millikan, R. *Phys. Rev.* **1923**, *22*, 1−23.